A Molecular-Dynamics Study of Size and Chirality Effects on Glass-Transition Temperature and Ordering in Carbon Nanotube-Polymer Composites

Marcello Malagù,* Alexey Lyulin, Elena Benvenuti, Angelo Simone

Molecular-dynamics simulations of single-walled carbon nanotubes (CNTs) embedded in a coarse-grained amorphous monodisperse polyethylene-like model system have been carried out. The roles of nanotube diameter and chirality on the physical and structural properties of the composite are thoroughly discussed for several CNTs with different diameter and chirality. It is shown that the glass-transition temperature of the polymer matrix increases with the diameter of the CNT while chirality effects are negligible. A denser and ordered layered region of polymer matrix is found in the vicinity of the nanotube surface. The density and ordering of this layer increases with the CNT diameter. All simulations indicate that chirality does not affect the atomic structure of the highly ordered layer surrounding the CNTs. Despite the simplicity of the polymer model, results of this study are qualitatively comparable with those obtained from experiments and numerical simulations that consider a chemically specific polymer matrix.

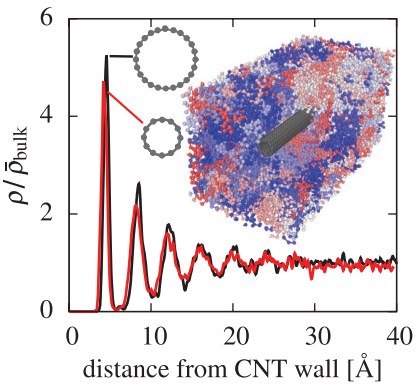

1. Introduction

When carbon nanotubes (CNTs) are used as inclusions in polymeric materials, important changes in the atomic structure of the hosting matrix can take place. Experimental evidence on a large class of CNT-polymer composites indicates that nanotubes can promote crystallization.[1–9] Despite the growing interest in carbon nanotube-polymer composites, CNT-induced effects on the polymer structure are still not well characterized due to the complexity of the interactions at the nanoscale.[10–13] Several factors can influence the nucleating effect of CNTs:[14] nanotube diameter and chirality, presence of surface functional groups, use of surfactants, CNT volume fraction, and type of polymer (it is worth mentioning that, besides CNT-induced crystallization, negligible[15] and anti-nucleation[16,17] effects have been observed in a small number of polymer types). Here, by using molecular-dynamics (MD) simulations, we present a preliminary study of CNT-induced ordering with a focus on the roles of CNT diameter and chirality.

The nucleation of a crystallized polymer layer around a nanotube is highly beneficial to the enhancement of the composite thermal and mechanical properties.[18–20] Although changes in the structure of the polymer matrix are limited to the nanoscale, their influence at the

M. Malagù, Dr. E. Benvenuti
Engineering Department
University of Ferrara
Via Saragat 1, 44122 Ferrara, Italy
E-mail: m.malagu@tudelft.nl
M. Malagù, Dr. A. Simone
Faculty of Civil Engineering and Geosciences
Delft University of Technology P.O. Box 5048, 2600 GA, Delft
The Netherlands
Dr. A. Lyulin
Department of Applied Physics
Eindhoven University of Technology P.O. Box 513, 5600 MB
Eindhoven, The Netherlands

macroscopic level is significant.[20–23] A detailed characterization of the atomic structure of the crystallized polymer layer, however, is not trivial. Being the nanotube size comparable to the characteristic length scale of the matrix atomic structure, the size of the CNT diameter might influence the ordering of the polymer chains. As observed experimentally from the analysis of crystallized polyethylene on different nanofillers[24] (single- and multiwalled CNTs, carbon nanofibers, and graphene), small-diameter fibers cause the polymer chains to align along their axis. In addition, molecular crystallization might also be influenced by the CNT chirality.[14]

The experimental quantification of structurally induced effects of the CNT on the polymer matrix is very difficult to accomplish due to the small size of the crystallized layer.[25] Moreover, it would be extremely challenging to isolate effects from other sources (e.g., preparation procedure and experimental technique). For these reasons, MD, which is here used to study structure and mobility of the polymer chains surrounding the nanotubes, has been typically employed. Minoia et al.[26] reported diameter effects on the structure and adhesion of single polyethylene chains on single-walled CNTs and negligible chirality effects. In contrast, Wei[27] observed chirality effects from MD simulations on single-walled CNTs surrounded by one layer of polyethylene chains. To investigate the more complex structure of a composite having a large number of polymer chains, Falkovich et al.[28] compared the ordering of an R-BAPB polyimide matrix in the vicinity of a flat graphene layer and a small diameter single-walled CNT. Their results show higher ordering in the case of the graphene sheet. However, their study does not provide a comprehensive description of diameter-induced modifications (only one nanotube was considered) and does not explore chirality effects. Furthermore, all the above results might be limited to the specific polymer considered in the simulations. Hence, a detailed and more fundamental understanding of CNT-induced effects and the interaction between polymer chains and filler is still lacking.

The purpose of this study is therefore twofold: to assess nanotube-induced effects on the atomic structure of the surrounding polymer matrix, and to provide a description of size and chirality effects that can be observed in a wide range of single-walled CNT-polymer composites. In the MD simulations, we employ a simple model of a CNT-polymer composite consisting of a single single-walled CNT embedded in a polymer matrix. We also avoid polymer chemistry-specific effects by using a simplified polyethylene-like coarse-grained (CG) model that has the added advantage of reducing the computational effort for the long relaxation time of the system –this simplified CG model is intended for the investigation of CNT-induced effects on an amorphous monodisperse polymer polyethylene-like matrix rather than on a specific polymer matrix. Diameter and chirality effects are here explored by means of a detailed fully atomistic single-walled CNT model. Non-bonded interactions are defined between nanotube and polymer chains and within the polymer chains.

To assess the influence of the nanotube-polymer interaction, the variation of the composite glass-transition temperature is discussed. Next, a comprehensive and detailed analysis of the structural properties of single-walled CNT-polymer composites is carried out by investigating density profile and ordering of the polymer chains around the nanotube. Throughout the paper, we qualitatively compare our results with experimental and modeling literature findings to validate the reliability of the atomistic model.

All the simulations and the corresponding results will help to elucidate nanotube-induced diameter and chirality effects at the level of the structure of the interface of the hosting polymer matrix. To the best of our knowledge, none of the previous studies in the literature provides such an extensive investigation and a basic understanding of single-walled CNT-effects in polymer-based composites.

2. Model and Simulation Details

Since we are interested in exploring features of an archetype single-walled CNT-polymer composite, a CG model is adopted for the polymer chains. Effects induced by the specific chemistry of the polymer matrix are therefore not considered. In view of the investigation of size and chirality effects, a fully atomistic representation of different single-walled CNTs is employed. Despite its simplicity, this atomistic model yields results in agreement with those from experiments and atomistic simulations with real polymers as discussed in the next section.

In the simulations, each polymer chain consists of 300 identical monomeric units, here referred to as beads. Assuming r as the distance between two beads, covalently bonded interactions are described by the interatomic potential

$$U(r) = -0.5KR_0^2 \ln\left[1-\left(\frac{r}{R_0}\right)^2\right] + 4\epsilon_p\left[\left(\frac{\sigma_p}{r}\right)^{12} - \left(\frac{\sigma_p}{r}\right)^6 + \frac{1}{4}\right] \quad (1)$$

The first term, which is attractive and defined according to the Finitely Extensible Nonlinear Elastic (FENE) potential,[29] depends on the stiffness K and the maximum elongation R_0 of the polymer bonds. The second term, which, conversely, is repulsive, is a truncated Lennard-Jones (LJ) potential defined in terms of beads characteristic length-scale σ_p and energy ε_p parameters. Although common

practice suggests the use of dimensionless LJ units for the quantities in (1), Kremer and Grest[29] suggested some values by comparing the dynamics of entangled FENE chains melts and real polymers. Accordingly, we take parameters σ_p, ε_p, K and R_0 equal to 5.1 Å, 0.8903 kcal mol^{-1}, $30\epsilon_p/\sigma_p^2$, and $1.5\sigma_p$, respectively. These values were suggested for amorphous monodisperse polyethylene-like systems. The interatomic potential (1) does not include bending and torsional contributions. Hence, the effect of the polymer chains flexibility on the physical properties of the composite is not examined in this work. The modified Morse potential[30] is employed to model the CNTs adopting the same parameters defined in our previous work.[31] Further, the 12-6 LJ potential has been considered for polymer-polymer and polymer-CNT non bonded interactions. In particular, the parameters σ_{pc} and ε_{pc} for the LJ interactions between polymer beads and CNT carbon atoms are calculated with the Lorentz–Berthelot rules

$$\sigma_{pc} = \frac{1}{2}\left(\sigma_p + \sigma_c\right) \quad \text{and} \quad \epsilon_{pc} = \sqrt{\epsilon_p\,\epsilon_c} \tag{2}$$

where σ_c and ε_c are the LJ parameters for CNT carbon atoms.[32]

The starting configuration of a CNT-polymer composite was generated by randomly packing stretched polymer chains in a large simulation box with one single-walled CNT at the center aligned in the z-axis—the Packmol package[33] was used for this task. The number of polymer chains, which depends on the nanotube diameter, corresponds to a nanotube volume ratio υ^{CNT} approximately equal to 0.6%[20,34] at 100 K and to a weight fraction w^{CNT} of ≈2% (see Tables 1 and 2). The initial configurations were relaxed at the rather high initial temperature of 800 K in an NVT ensemble for 0.5 ns. Since the volume of the CNT and the density of polymer at 800 K are known, the approximated volume of the composite at that temperature can be estimated. This information was used in the next step where the size of the simulation box was reduced until the desired volume was reached. Each system was further relaxed at 800 K in an NPT ensemble at 0 atm—indistinguishable from 1 atm since pressure fluctuations are in the range of about ±50 atm—for 10 ns, a period that was long enough to reach equilibration (checked by measuring the variation of the energy). This initialization phase, used to reach the equilibrium volume of the composite, was preferred over a single NPT ensemble since it leads to a shorter computational time and equivalent equilibrated configurations.

Table 1. Diameter d of the embedded armchair single-walled CNTs and nanotube volume fraction υ^{CNT} and weight fraction w^{CNT} in the (n,n)-polymer composites.

	(6,6)-polymer	(8,8)-polymer	(10,10)-polymer	(12,12)-polymer
d [Å]	8.14	10.86	13.57	16.28
υ^{CNT} [%]	0.64	0.62	0.62	0.62
w^{CNT} [%]	2.09	2.00	1.98	1.95

Table 2. Diameter d of the embedded zigzag single-walled CNTs and nanotube volume fraction υ^{CNT} and weight fraction w^{CNT} in the (n,o)-polymer composites.

	(10,0)-polymer	(14,0)-polymer	(17,0)-polymer	(21,0)-polymer
d [Å]	7.83	10.97	13.32	16.45
υ^{CNT} [%]	0.63	0.62	0.62	0.62
w^{CNT} [%]	2.08	2.00	1.98	1.95

Finally, all systems were further cooled down in an NPT ensemble at a cooling rate of 0.1 K ps^{-1} (see Figure 1 for a typical snapshot of an (8,8)-polymer composite at 100 K).

All simulations have been performed using the Large-scale Atomic/Molecular Massively Parallel Simulator (LAMMPS) software package.[35] We choose periodic boundary conditions in all three directions. The Newton's equations of motion were integrated with the velocity Verlet algorithm using a time step of 1 fs. The Nosé–Hoover thermostat and barostat were used. For each system, three different initial configurations were generated and the corresponding results were averaged. The LAMMPS input scripts can be downloaded from the authors' website.

Next, four armchair ((6,6), (8,8), (10,10) and (12,12)) and four zigzag ((10,0), (14,0), (17,0) and (21,0)) nanotubes with different diameters are used to assess chirality and size effects. Throughout the paper, the standard notation employing the couple of integers (n, m) to describe single-walled CNTs[36] is adopted. Moreover, the notation (n,m)-polymer denotes a polymer composite with an (n, m) single-walled CNT. The diameter of the nanotubes was calculated as

$$d = \frac{a_{cc}\sqrt{3\left(n^2 + m^2 + nm\right)}}{\pi} + t \tag{3}$$

where a_{cc}=1.421 Å is the length of the carbon-carbon bonds and t=3.4 Å the nanotube thickness.[37]

3. Results and Discussion

3.1. Glass-Transition Temperature

In nanocomposites, the glass-transition temperature (T_g) is one of the simplest way to characterize the interaction

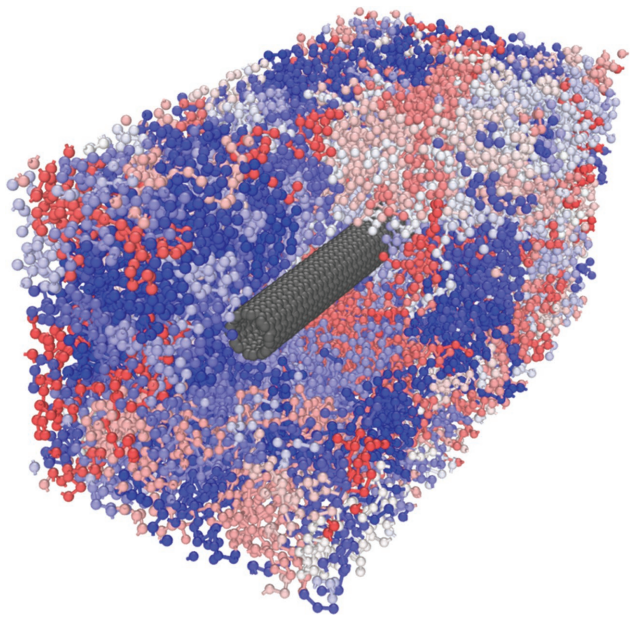

Figure 1. Illustration of an (8,8)-polymer composite equilibrated at 100 K (part of the polymer matrix has been removed for better visualization of the embedded nanotube). Polymer chains are displayed in different colors, the nanotube in gray.

between polymer chains and filler. Figure 2 shows the density-temperature curves for the bulk material and an (8,8)-polymer composite. The bulk T_g was estimated as 200.9 K and corresponds to the dimensionless quantity 0.448~ε_p/k_B, with k_B the Boltzmann constant. This result is in good agreement with theoretical[38] and numerical[39–41] estimates for FENE polymer melts—these values

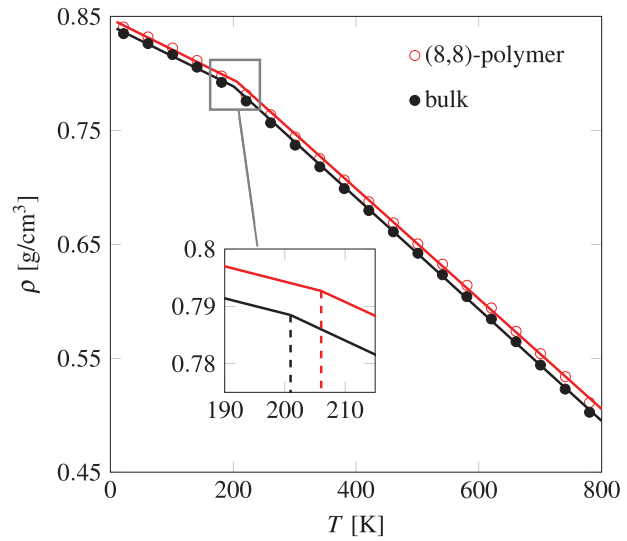

Figure 2. Density–temperature curves for bulk polymer and an (8,8)-polymer composite. Solid lines indicate linear fits to calculate the glass-transition temperature. Dashed lines denote the estimated value of T_g.

vary between 0.43 and 0.47 ε_p/k_B. The obtained T_g, however, is lower than that for real polyethylene (between 220 and 280 K).[42–46] Nevertheless, a quantitative comparison between the estimated glass-transition temperatures and those for real polyethylene is beyond the scope of the this study and the model employed in our simulations. The CG model for the polymer chains is employed to provide general insight into a wide range of polymer-based materials. Indeed, as discussed next, the obtained results are in line with those from real composites. As depicted in Figure 2, the glass-transition temperature increases to T_g = 206.0 K for the case of the (8,8)-polymer composite denoting attractive interactions between the nanotube and the surrounding polymer chains.[47] More precisely, since the glass-transition temperature of the composite is higher than that of the bulk matrix, CNT-polymer interactions are stronger than those between polymer beads. Noteworthy, the variation of T_g is comparable with the variation obtained from experimental and numerical studies on real single-walled CNT-polymer composites. Liang and Tjong[48] estimated the glass-transition temperature of CNT-low density polyethylene composites about 10 K higher than that for pure polymer matrix. Grady et al.,[49] from experiments on CNT-polystyrene composites with a nanotube weight fraction varying between 1% and 30%, reported T_g values 6–7 K higher than those for pure polystyrene. Sterzyński et al.[50] obtained the T_g of polyvinyl chloride matrix about 9 K lower than that of the corresponding CNT composite with a CNT concentration of 0.01–0.02 wt%. For poly(methyl methacrylate) composites an increase of about 2 K was observed with a content of CNTs of about 0.5 wt%.[51] Wei et al.,[52] using MD simulations of single-walled CNT-polyethylene composites, estimated T_g about 20 K higher than that of the bulk material.

The influence of the nanotube atomic structure on the glass-transition temperature was investigated as well. In Figure 3a, size and chirality effects on T_g are depicted for all simulated CNT-polymer composites.

3.1.1. Size Effects

The composite glass-transition temperature, while remaining higher than the bulk T_g, clearly increases with the curvature of the nanotube (Figure 3a). This can be explained by considering that the number of non-bonded interactions between polymer beads and nanotube atoms increases with decreasing d[53] as shown in Figure 3b. Consequently, the mobility of the polymer chains surrounding the nanotubes decreases.

It is worth mentioning that also the value of the CNT weight fraction can influence T_g. Nevertheless, as indicated in Tables 1 and 2, the variation of w^{CNT} is small, especially if compared with the changes in the CNT

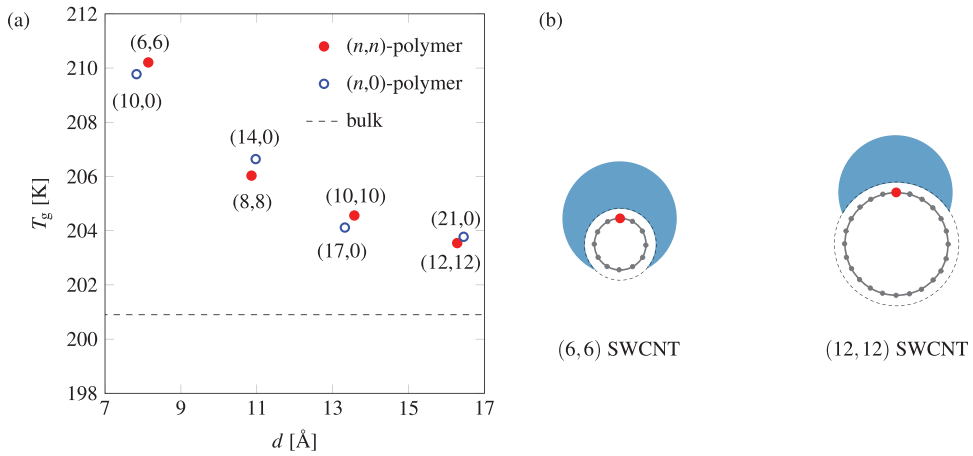

Figure 3. a) Glass-transition temperature of (*n*, *n*) armchair and (*n*,0) zigzag single-walled CNT-polymer composites as a function of the nanotube diameter *d* compared to the bulk glass-transition temperature. b) Schematic of the interaction region (blue) of a single-walled CNT atom (red) with the surrounding polymer.[53]

diameter. Therefore, it is reasonable to assume that the trend of the composite glass-transition temperature T_g is mainly caused by the variation of the nanotube diameter *d*.

3.1.2. Chirality Effects

As depicted in Figure 3 a, the estimated values of T_g for armchair and zigzag composites differ by less than 1%. Since armchair and zigzag configurations represent the two extremes, minimum and maximum value, respectively, in terms of chirality, these results suggest that chirality-induced effects on T_g are negligible.

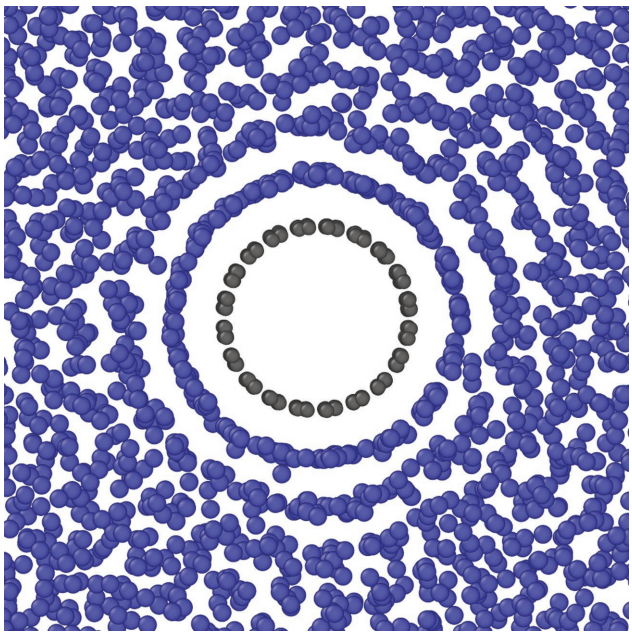

Figure 4. Snapshot of an (8,8)-polymer composite cross section at 100 K (monomer beads in blue, single-walled CNT carbon atoms in gray).

3.2. Density Profiles

Typically, in confined geometries and polymer composites with particle inclusions, a better packing of monomer units is observed around the interface.[47,54] As depicted in Figure 4, this is also the case for the single-walled CNT-polymer composites considered in this work. Concentric wall-induced layers can be identified around the nanotube. A detailed investigation of the density profile was therefore carried out to understand structural changes in the polymer matrix in the vicinity of the nanotube.

To start with, the evolution of the density profile at different temperatures has been examined. As illustrated in Figure 5, the number of wall-induced layers and their density increase while cooling the system. The intensity of the peaks is higher close to the nanotube surface and it decays until the composite density equals that of the bulk. Noteworthy, the peak-to-peak distance remains constant and equal to about σ_p at all temperatures. This suggests that the bonds connecting two polymer beads in different layers (whose equilibrium distance is $0.97\sigma_p$) are mainly orthogonal to the nanotube surface and to its longitudinal axis. Consequently, a higher ordering of the monomers, which increases by decreasing the temperature, is observed around the nanotube (this will be discussed in more detail in the next section).

3.2.1. Size Effects

Figure 6 shows a comparison of the density profiles for different armchair composites at (a) 800 and (b) 100 K. Similar profiles are observed for all the examined

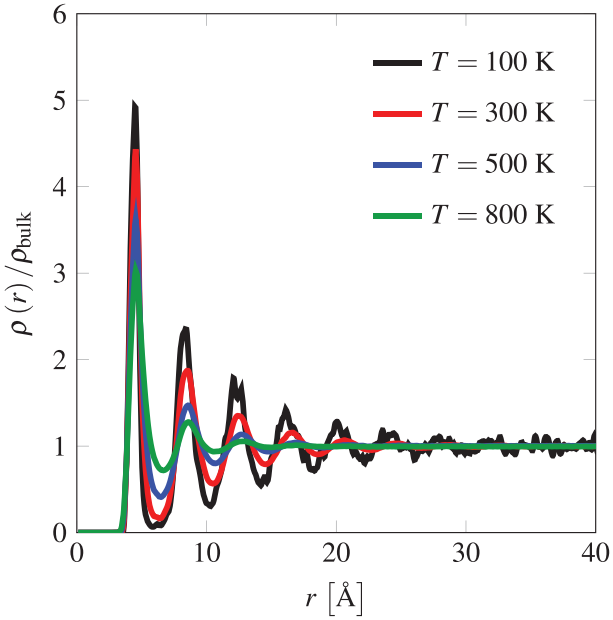

Figure 5. Density of an (8,8)-polymer composite at different temperatures as a function of distance r from the nanotube wall (all curves have been normalized with respect to the bulk density ρ_{bulk} at the corresponding temperature).

armchair composites. The number of layers and the peak-to-peak distance is the same. Moreover, the thickness of the perturbed region of polymer matrix (i.e., the interphase) does not change with the diameter of the nanotube—analogous results were obtained by Brown et al.[55] with MD simulations on a polymer matrix with spherical inclusions—and is about 25 Å. Therefore, as schematically shown in Figure 7, for CNT-polymer composites with equal υ^{CNT}, the volume fraction of such interphase layer increases by decreasing the diameter of the nanotube. This size effect might have a role in the trend of T_g observed in Section 3.1.1 since the glass-transition temperature of the highly ordered polymer region is higher than that of the amorphous bulk polymer. Nonetheless, the density of the wall-induced layers increases with the nanotube diameter—weaker maxima and minima can be noticed for smaller nanotubes. This is in agreement with the results from Falkovich et al.[28] obtained with MD simulations of R-BAPB composites with graphene and a (5,5) CNT.

3.2.2. Chirality Effects

Chirality effects on monomer packing are negligible. This can be deduced from Figure 8 where the density profiles of composites with single-walled CNT of comparable diameter ((12,12) armchair and (21,0) zigzag) are shown. Analogous conclusions hold for the other composites.

3.3. Ordering of Monomers

Based on the analysis of the density profile, a higher ordering of the polymer bonds was observed in the vicinity of the nanotubes. However, the previous results do not provide a comprehensive description of the changes that nanotubes induce in the matrix monomer structure. In this section we carry out a detailed investigation into the orientation of the polymer bonds with respect to the nanotube longitudinal axis and surface.

Similar to Falkovich et al.[28] we employed histograms showing the probability P of the orientation of the polymer bonds as a function of the distance from the nanotube wall. The monomer orientation is measured according to the angles ϕ and θ between the polymer bonds and the nanotube axis and surface, respectively. The results are derived by averaging the bond orientation sampled every 5 ps within a time interval of 10 ns. The

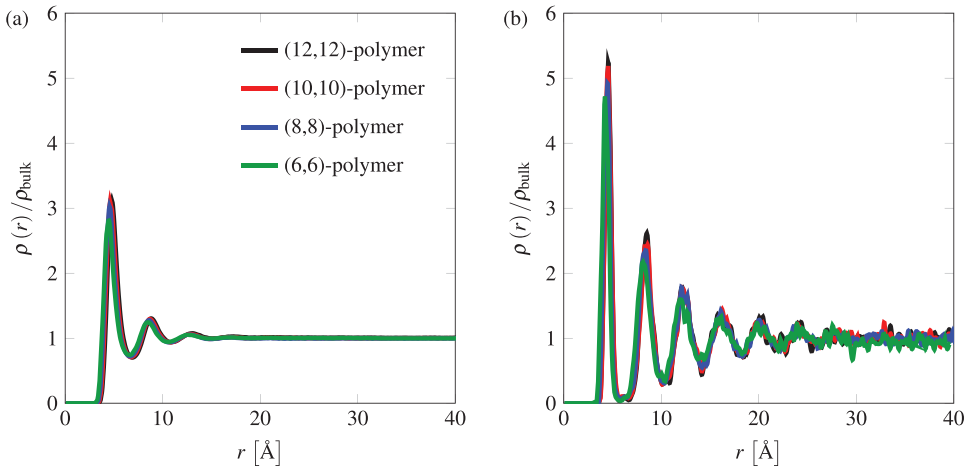

Figure 6. Density profile for different armchair composites at a) 800 K and b) 100 K as a function of distance r from the single-walled CNT wall (all curves are normalized with respect to the bulk density ρ_{bulk} at the corresponding temperature).

Macromolecular Journals
Macromol. Theory Simul. **2016**, DOI: 10.1002/mats.201600041

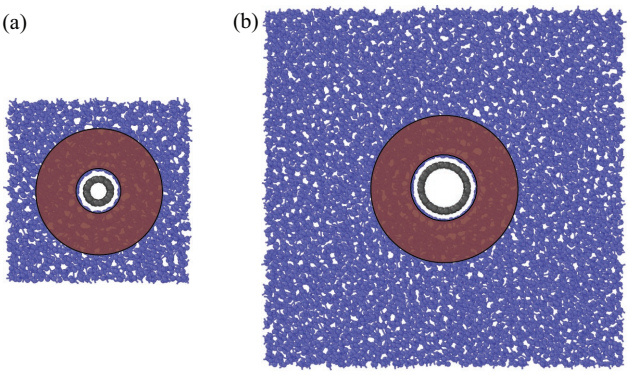

Figure 7. Schematic showing the region of polymer with higher ordering (highlighted in brown) in a) (6,6) and b) (12,12) single-walled CNT-polymer composites with υ^{CNT} = 0.6%. Since the thickness of the perturbed polymer phase, about 25 Å, does not change with the nanotube diameter *d*, its volume fraction increases by decreasing *d*.

bin size of the histograms was chosen equal to 1° for both angles ϕ and θ and 1 Å for the distance *r*.

The ordering of the monomers was first assessed in a polymer matrix system without CNT. In this case, we estimated the probability of the bonds to align with the *x*-axis of the simulation unit cell (analogous results were produced estimating *P* with respect to the *y*- and *z*-axes). As depicted in Figure 9, the histogram evaluated at 100 K does not show preferential orientations of the polymer bonds. Therefore, in absence of CNTs, the matrix is amorphous. In contrast to this, as illustrated in Figures 10 a and 11 a for an (8,8)-polymer composite, higher ordering is already visible at 800 K in the polymer interfacial layer ($r \approx 4$–5 Å). In particular, while the ordering with respect to the nanotube axis is very mild, most of the polymer bonds are nearly parallel to the nanotube surface. By decreasing the temperature, the ordering increases and more ordered layers form (see Figure 10 b–d and 11 b–d).

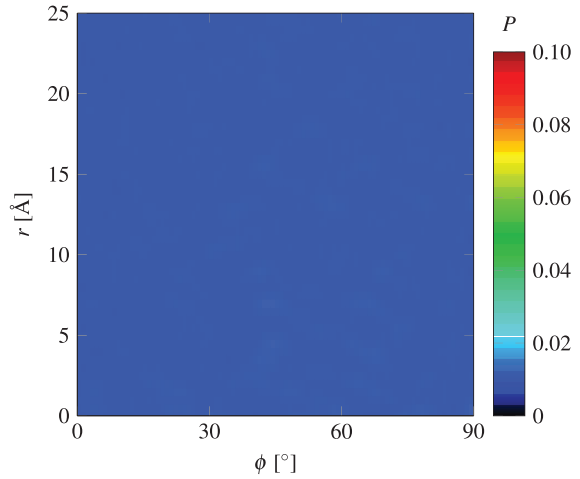

Figure 9. Probability *P* of the angle ϕ between the polymer bonds and the *x*-axis of the unit cell for a pure polymer matrix system at 100 K. Histograms at higher temperatures are analogous, indicating no high ordering for the pure polymer matrix.

In the first layer, located between 4 and 5 Å from the nanotube wall, the probability of orientation along the nanotube axis presents a high peak between 0 and 5° and, especially at low temperatures, lower peaks at larger values of ϕ. Regarding θ, we observe only one peak at 0°–10°. This suggests that polymer bonds at the interface, while being parallel to the nanotube surface, are preferentially aligned with the nanotube axis. Conversely, in the second layer positioned at 6–7 Å, polymer bonds are mainly orthogonal to the nanotube surface since the angle distribution peaks are at 70°–90° for ϕ and θ. This pattern of alternating layers of parallel and orthogonal bonds repeats while moving far from the interface. However, the ordering decays with *r* since the influence of the nanotube over the polymer atoms vanishes. These results indicate the nucleation of an ordered region that has been

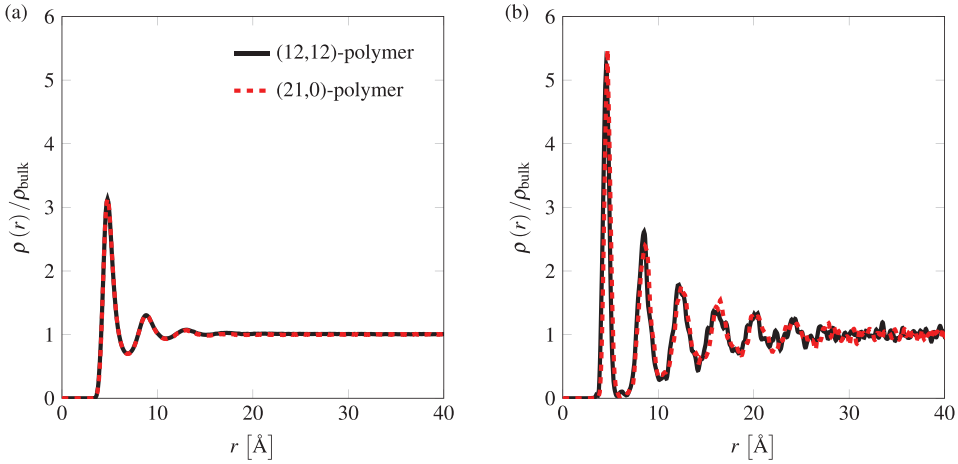

Figure 8. Density profile for (12,12) armchair and (21,0) zigzag single-walled CNT-polymer composites at a) 800 K and b) 100 K as a function of distance *r* from the nanotube wall (all curves are normalized with respect to the bulk density ρ_{bulk} at the corresponding temperature).

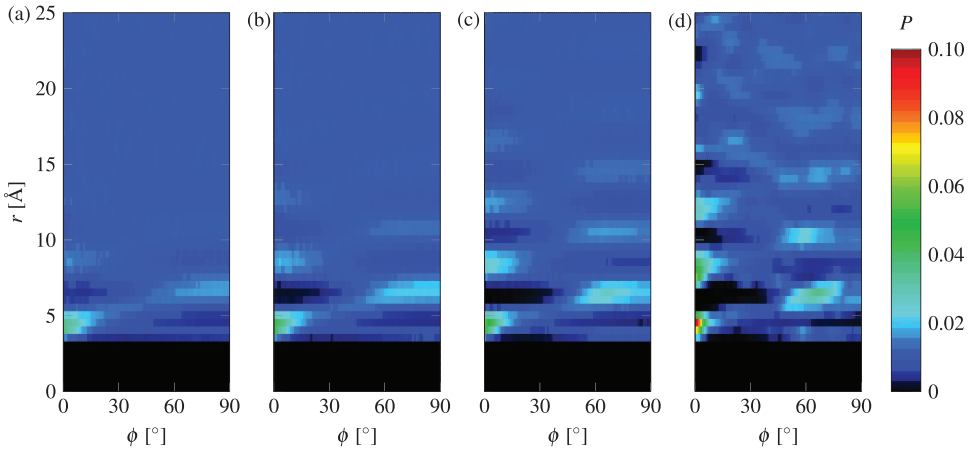

Figure 10. Probability *P* of the angle ϕ between the polymer bonds and the longitudinal axis of an (8,8) single-walled CNT at a) 800, b) 500, c) 300, and d) 100 K: the nanotube initiates high ordering at the interface. The ordering increases while cooling the system.

experimentally observed in several real single-walled CNT-polymer composites,[14] as widely reported for CNT-polyethylene.[6,7,12,56–58] Analogous observations were made for other semi-crystalline polymers such as isotactic polypropylene,[2,34,59] poly(vinylidene difluoride),[60,61] and poly(vinyl alcohol).[18,62] Based on Raman spectroscopy on CNT-poly(ε-caprolactone), Chatterjee and co-workers[21] showed the formation of an ordered polymer structure oriented along the surface of the nanotubes. Regarding amorphous polymers, Dingemans and co-workers[20,63,64] reported the growth of a crystalline domain of polyetherimide matrix along the CNT surface.

3.3.1. Size Effects

A quantitative assessment of size effects on the monomer ordering is shown in Figure 12 based on the estimation of the fraction $\psi_\alpha(r)$ of polymer bonds not exceeding a given angle α with the nanotube axis. The results have been reported only for (6,6)-polymer and (12,12)-polymer composites. At 800 and 100 K, the fraction ϕ_α of monomer bonds shows a high peak at r = 4–5 Å and then decreases moving far from the nanotube surface. This denotes the higher ordering of the polymer matrix in the vicinity of the nanotube as previously discussed. At 800 K size effects are minimal. On the contrary, at 100 K, stronger ordering is noticed for the composite with the nanotube with larger diameter. Consequently, increasing the nanotube curvature hinders the ordering of the surrounding polymer chains. For temperatures between 800 and 100 K (e.g., 300 K) we observed results in between those shown in Figure 12. Minoia et al.,[26] performing MD simulations at 300 K of single polymer chains on single-walled CNTs, related this diameter effect to the higher binding energy observed in the case of nanotube with lower curvature as more bending of the polymer chains is required to

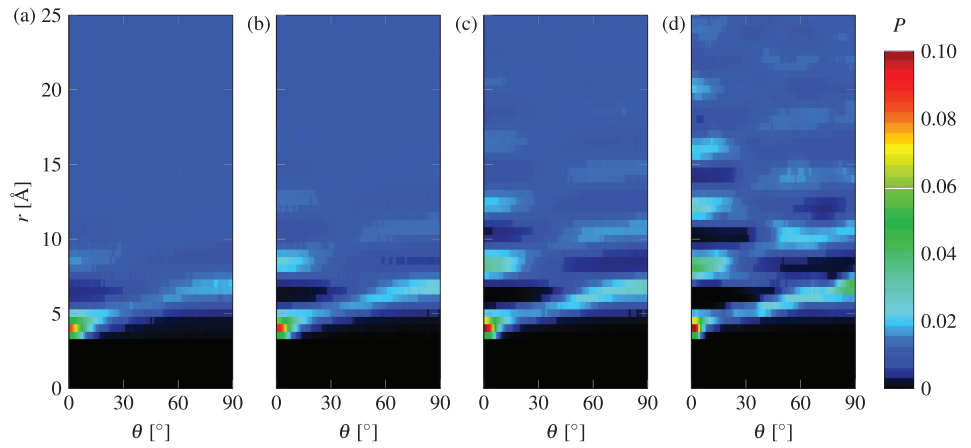

Figure 11. Probability *P* of the angle θ between the polymer bonds and the surface of an (8,8) single-walled CNT at a) 800, b) 500, c) 300, and d) 100 K: the nanotube initiates high ordering at the interface. The ordering increases while cooling the system.

Macromolecular Journals
Macromol. Theory Simul. **2016**, DOI: 10.1002/mats.201600041

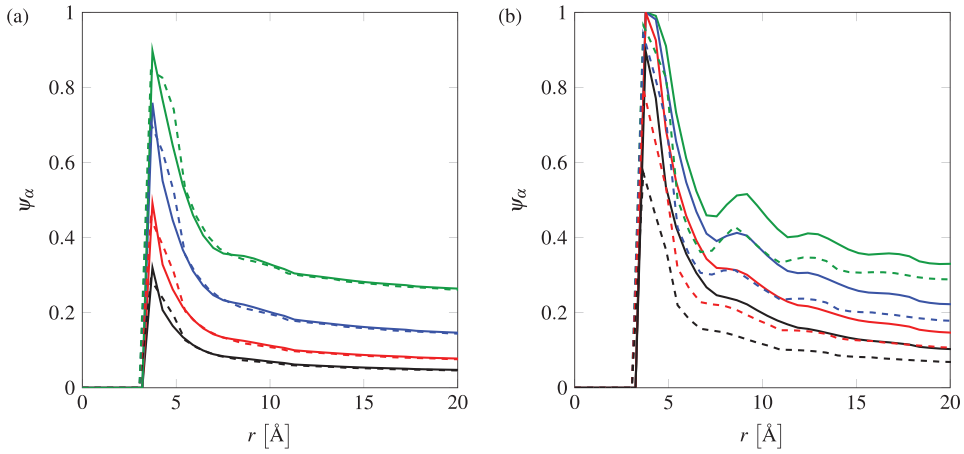

Figure 12. Fraction ϕ_α of monomer bonds at a distance r from the nanotube wall and at an angle $\theta < \alpha$ to the axis of armchair (12,12) (solid lines) and (6,6) (dashed lines) single-walled CNTs at a) 800 and b) 100 K. The angle α is equal to 2.5° (black lines), 5° (red lines), 10° (blue lines) , and 20° (green lines).

maintain their atoms in close contact with small diameter CNTs. Although a bending contribution is not explicitly implemented in the FENE potential, the repulsive term in (1) provides flexural stiffness to the polymer chains. Therefore, despite the increase of CNT-polymer interaction for smaller nanotubes (as illustrated in Figure 3 b), higher ordering is observed when the curvature of the nanotube decreases.

3.3.2. Chirality Effects

Figure 13 shows that the $\psi_\alpha(r)$ profiles for (12,12) armchair single-walled CNTs are closely akin to those obtained with (21,0) zigzag nanotubes. The small differences in $\psi_\alpha(r)$ arise from the size effects—the (21,0) zigzag single-walled CNT, having a larger diameter, leads to a slightly higher ordering. Therefore, as observed for the variation of T_g and the density profile, chirality effects in armchair, and zigzag composites are negligible.

4. Conclusions

We assessed diameter and chirality effects on physical and structural properties of single-walled CNT-polymer composites by means of MD simulations. Attractive non-bonded interactions between the polymer matrix and the CNT yield a composite glass-transition temperature higher than that of the bulk matrix and a highly ordered layer of polymer chains in the vicinity of the nanotube wall. In particular, our simulations revealed that density and monomer ordering of the polymer matrix rapidly increase close to the nanotube surface. The main conclusions regarding size and chirality effects are summarized below.

Size Effects: The glass-transition temperature of the composite increases with the curvature of the nanotube while the thickness of the highly ordered layer surrounding the nanotubes does not change with the size of the nanotube. Nevertheless, the nanotube diameter influences its density

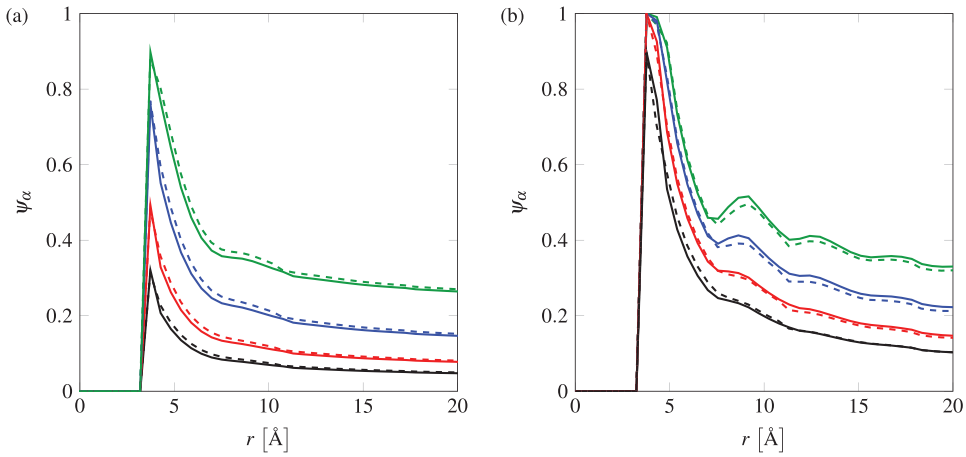

Figure 13. Fraction ϕ_α of monomer bonds at a distance r from the nanotube wall and at an angle $\theta < \alpha$ to the axis of (12,12) armchair (solid lines) and (21,0) zigzag (dashed lines) single-walled CNTs at a) 800 and b) 100 K. The angle α is equal to 2.5° (black lines), 5° (red lines), 10° (blue lines), and 20° (green lines).

profile and ordering. Namely, increasing the nanotube diameter increases the ordering of the polymer chains around the nanotube surface. Therefore, the results show that higher glass-transition temperature T_g does not lead to higher ordering in the polymer. The estimated values of T_g depend on the number of CNT-polymer interactions, while the ordering of the polymer chains depends on their possibility to maintain the monomers in close contact with the nanotube atoms.

Chirality Effects: The effects induced by the nanotube chirality, on the contrary, were negligible, with the results obtained for armchair and zigzag single-walled CNTs with similar diameter showing only minor differences. Hence, our findings suggest that the orientation of the periodic atomic structure of the nanotube along its longitudinal axis influences neither the density profile nor the ordering of the highly ordered polymer layer.

The relevance of our results has to be considered in the light of the characterization and design of CNT-polymer materials. Structural changes induced by nanotubes embedded in a polymer matrix might have interesting implications for physical and mechanical properties of the composite. More specifically, as the ordering of the polymer chains around the nanotube increases with its diameter, the role of size effects on the macroscopic mechanical properties of CNT-polymer composites might be significant.

Although a direct and quantitative comparison between the proposed MD model and real CNT-polymer composites was difficult and beyond the scope this work, the obtained results were meaningful. Indeed, despite the simplicity of the atomistic representation employed for the polymer chains and the composite, the results are in good agreement with experimental and modeling literature findings that show nucleation of a crystallized or highly ordered polymer layer around the nanotube surface.

Acknowledgement: The research leading to these results received funding from MIUR (Fondo Giovani 2011) and the European Research Council under the European Union's Seventh Framework Programme (FP7/2007-2013)/ERC Grant agreement no. 617972. The authors are grateful to Prof. T. J. Dingemans for helpful comments on this work.

Received: May 11, 2016; Revised: August 22, 2016; Published online: ; DOI: 10.1002/mats.201600041

Keywords: carbon nanotubes; crystallization; molecular dynamics; polymer; size effects

[1] D. M. Dean, L. Rebenfeld, R. A. Register, B. S. Hsiao, *J. Mater. Sci.* **1998**, *33*, 4797.
[2] E. Assouline, A. Lustiger, A. H. Barber, C. A. Cooper, E. Klein, E. Wachtel, H. D. Wagner, *J. Polym. Sci., Part B: Polym. Phys.* **2003**, *41*, 520.
[3] A. R. Bhattacharyya, T. V. Sreekumar, T. Liu, S. Kumar, L. M. Ericson, R. H. Hauge, R. E. Smalley, *Polymer* **2003**, *44*, 2373.
[4] V. E. Yudin, V. M. Svetlichnyi, A. N. Shumakov, D. G. Letenko, A. Y. Feldman, G. Marom, *Macromol. Rapid Commun.* **2005**, *26*, 885.
[5] K. A. Anand, U. S. Agarwal, R. Joseph, *Polymer* **2006**, *47*, 3976.
[6] L. Li, Y. Yang, G. Yang, X. Chen, B. S. Hsiao, B. Chu, J. E. Spanier, C. Y. Li, *Nano Lett.* **2006**, *6*, 1007.
[7] L. Li, C. Y. Li, C. Ni, *J. Am. Chem. Soc.* **2006**, *128*, 1692.
[8] M. L. Minus, H. G. Chae, S. Kumar, *Polymer* **2006**, *47*, 3705.
[9] E.-C. Chen, T.-M. Wu, *Polym. Degrad. Stab.* **2007**, *92*, 1009.
[10] A. H. Barber, S. R. Cohen, H. D. Wagner, *Appl. Phys. Lett.* **2003**, *82*, 4140.
[11] J. Shen, W. Huang, L. Wu, Y. Hu, M. Ye, *Compos. Sci. Technol.* **2007**, *67*, 3041.
[12] R. Haggenmueller, J. E. Fischer, K. I. Winey, *Macromolecules* **2006**, *39*, 2964.
[13] S. V. Larin, S. G. Falkovich, V. M. Nazarychev, A. A. Gurtovenko, A. V. Lyulin, S. V. Lyulin, *RSC Adv.* **2014**, *4*, 830.
[14] E. D. Laird, C. Y. Li, *Macromolecules* **2013**, *46*, 2877.
[15] H. W. Goh, S. H. Goh, G. Q. Xu, K. P. Pramoda, W. D. Zhang, *Chem. Phys. Lett.* **2003**, *379*, 236.
[16] T. Chatterjee, A. T. Lorenzo, R. Krishnamoorti, *Polymer* **2011**, *52*, 4938.
[17] H. Z. Geng, R. Rosen, B. Zheng, H. Shimoda, L. Fleming, J. Liu, O. Zhou, *Adv. Mater.* **2002**, *14*, 1387.
[18] M. Cadek, J. N. Coleman, V. Barron, K. Hedicke, W. J. Blau, *Appl. Phys. Lett.* **2002**, *81*, 5123.
[19] J. N. Coleman, M. Cadek, K. P. Ryan, A. Fonseca, J. B. Nagy, W. J. Blau, M. S. Ferreira, *Polymer* **2006**, *47*, 8556.
[20] M. Hegde, U. Lafont, B. Norder, S. J. Picken, E. T. Samulski, M. Rubinstein, T. Dingemans, *Macromolecules* **2013**, *46*, 1492.
[21] T. Chatterjee, C. A. Mitchell, V. G. Hadjiev, R. Krishnamoorti, *Adv. Mater.* **2007**, *19*, 3850.
[22] G. Gkikas, N.-M. Barkoula, A. S. Paipetis, *Composites, Part B* **2012**, *43*, 2697.
[23] X.-Q. Liu, W. Yang, B.-H. Xie, M.-B. Yang, *Mater. Des.* **2012**, *34*, 355.
[24] L. Li, B. Li, M. A. Hood, C. Y. Li, *Polymer* **2009**, *50*, 953.
[25] H. Uehara, K. Kato, M. Kakiage, T. Yamanobe, T. Komoto, *J. Phys. Chem. C* **2007**, *111*, 18950.
[26] A. Minoia, L. Chen, D. Beljonne, R. Lazzaroni, *Polymer* **2012**, *53*, 5480.
[27] C. Wei, *Nano Lett.* **2006**, *6*, 1627.
[28] S. G. Falkovich, S. V. Larin, A. V. Lyulin, V. E. Yudin, J. M. Kenny, S. V. Lyulin, *RSC Adv.* **2014**, *4*, 48606.
[29] K. Kremer, G. S. Grest, *J. Chem. Phys.* **1990**, *92*, 5057.
[30] T. Belytschko, S. P. Xiao, G. C. Schatz, R. S. Ruoff, *Phys. Rev. B* **2002**, *65*, 235430.
[31] M. Malagù, E. Benvenuti, A. Simone, *Eur. J. Mech. A Solids* **2015**, *54*, 160.
[32] D. W. Brenner, *Phys. Rev. B* **1990**, *42*, 9458.
[33] L. Martínez, R. Andrade, E. G. Birgin, J. M. Martínez, *J. Comput. Chem.* **2009**, *30*, 2157.
[34] B. P. Grady, F. Pompeo, R. L. Shambaugh, D. E. Resasco, *J. Phys. Chem. B* **2002**, *106*, 5852.
[35] S. Plimpton, *J. Comput. Phys.* **1995**, *117*, 1.
[36] M. S. Dresselhaus, G. Dresselhaus, P. C. Eklund, A. M. Rao, in, *The Physics of Fullerene-Based and Fullerene-Related Materials* (Ed: W. Andreoni), Springer, Dordrecht, **2000**, pp. 331.
[37] Y. Huang, J. Wu, K.-C. Hwang, *Phys. Rev. B* **2006**, *74*, 245413.
[38] J. Rottler, M. O. Robbins, *Phys. Rev. E* **2003**, *68*, 011507.

[39] J. Buchholz, W. Paul, F. Varnik, K. Binder, *J. Chem. Phys.* **2002**, *117*, 7364.
[40] M. Asai, M. Shibayama, Y. Koike, *Macromolecules* **2011**, *44*, 6615.
[41] C. Batistakis, M. A. J. Michels, A. V. Lyulin, *Macromolecules* **2014**, *47*, 4690.
[42] J. Brandrup, E. H. Immergut, Polymer Handbook, 3rd ed., John Wiley & Sons, Chichester, **1989**.
[43] K. F. Mansfield, D. N. Theodorou, *Macromolecules* **1991**, *24*, 6283.
[44] J. Han, R. H. Gee, R. H. Boyd, *Macromolecules* **1994**, *27*, 7781.
[45] R. H. Boyd, R. H. Gee, J. Han, Y. Jin, *J. Chem. Phys.* **1994**, *101*, 788.
[46] R. H. Gee, R. H. Boyd, *Comput. Theor. Polym. Sci.* **1998**, *8*, 93.
[47] F. W. Starr, T. B. Schrøder, S. C. Glotzer, *Macromolecules* **2002**, *35*, 4481.
[48] G. D. Liang, S. C. Tjong, *Mater. Chem. Phys.* **2006**, *100*, 132.
[49] B. P. Grady, A. Paul, J. E. Peters, W. T. Ford, *Macromolecules* **2009**, *42*, 6152.
[50] T. Sterzyński, J. Tomaszewska, K. Piszczek, K. Skórczewska, *Compos. Sci. Technol.* **2010**, *70*, 966.
[51] E. Logakis, C. Pandis, P. Pissis, J. Pionteck, P. Pötschke, *Compos. Sci. Technol.* **2011**, *71*, 854.
[52] C. Wei, D. Srivastava, K. Cho, *Nano Lett.* **2002**, *2*, 647.
[53] Z. Q. Zhang, D. K. Ward, Y. Xue, H. W. Zhang, M. F. Horstemeyer, *ISRN Mater. Sci.* **2011**, *2011*, 1.
[54] J. Baschnagel, F. Varnik, *J. Phys.: Condens. Matter* **2005**, *17*, R851.
[55] D. Brown, V. Marcadon, P. Mele, N. D. Alberola, *Macromolecules* **2008**, *41*, 1499.
[56] Q. Zhang, S. Rastogi, D. Chen, D. Lippits, P. J. Lemstra, *Carbon* **2006**, *44*, 778.
[57] Q. Zhang, D. R. Lippits, S. Rastogi, *Macromolecules* **2006**, *39*, 658.
[58] L. Zhang, T. Tao, C. Li, *Polymer* **2009**, *50*, 3835.
[59] N. Ning, W. Zhang, J. Yan, F. Xu, C. Tang, Q. Fu, *J. Mater. Res.* **2012**, *27*, 2812.
[60] N. Levi, R. Czerw, S. Xing, P. Iyer, D. L. Carroll, *Nano Lett.* **2004**, *4*, 1267.
[61] S. Yu, W. Zheng, W. Yu, Y. Zhang, Q. Jiang, Z. Zhao, *Macromolecules* **2009**, *42*, 8870.
[62] F. Zhang, H. Zhang, Z. Zhang, Z. Chen, Q. Xu, *Macromolecules* **2008**, *41*, 4519.
[63] M. Hegde, U. Lafont, B. Norder, E. T. Samulski, M. Rubinstein, T. J. Dingemans, *Polymer* **2014**, *55*, 3746.
[64] M. Hegde, E. T. Samulski, M. Rubinstein, T. J. Dingemans, *Compos. Sci. Technol.* **2015**, *110*, 176.